Fusing Landsat-5/TM Imagery and Shaded Relief Maps in Tectonic and Geomorphic Mapping: Lesvos Island, Greece

Nikolaos A. Soulakellis, Irwin D. Novak, Nikolaos Zouros, Paul Lowman, and Jacob Yates

Abstract

The significance of both solar elevation angle and azimuth are critical elements for examining Earth observation datasets. Illumination angle is a crucial parameter affecting the appearance of the topographically related and dependent features. Therefore, an improved methodology of data fusion for tectonic and geomorphic mapping is needed to augment the traditional false color composite analysis. A long-standing problem in such applications is the bias introduced by illumination geometry, specifically sun elevation and azimuth. A Landsat-5 image of Lesvos Island, Greece, was combined with digital elevation models to produce fused images with a wide range of illumination azimuths and elevation in a GIS environment. Sixteen combinations of sun elevation angle (using 15° and 30°) paired with azimuth (0° to 360° at 45° increments) were considered. This new technique compensates for local conditions such as generally cloudy winters which make it difficult to obtain images with low sun elevation or images of eroded landforms with subdued geomorphic expression. The resulting fused images combine the tonal information and high spatial resolution of Landsat with the strong topographic rendition of digital elevation models. Well-known faults, with more or less significant expression on the surface known from previous image interpretation and fieldwork, are more easily identifiable. Shaded relief maps produced by applying the lower illumination angle in combination with an azimuth perpendicular to the fault orientation produced the best results. Additionally, previously unknown linear and circular features, e.g., calderas, were represented in the low illumination angle image, independent of its azimuth. Fused images will be further combined with geologic and seismicity maps to study problems such as location of the Anatolian Plate's boundaries and their nature (sharp or diffuse).

Introduction

One of the earliest applications of widely available orbital imagery from Landsat-1 was in the study of lineaments, straight or gently curved linear geomorphic features, such as stream segments or lakes, often of regional extent (Wise, 1974; O'Leary *et al.*, 1976). First recognized by W.H. Hobbs early in the 20th Century, and long before even air photos were available, the field of basement tectonics, as it became known, was enormously stimulated by orbital methods (Lowman, 2002). Following conventional practice for air photo interpretation, the use of "lineament" excludes along-strike features such as dipping sedimentary strata (Lattman, 1958). Most lineaments, thus defined, have been found in the field to be fractures (faults or joint systems) or dikes following such fractures. In areas of high topographic relief, straight or nearly straight lineaments must have steep or vertical dips. The term lineament is sometimes used for broad linear zones of faults, igneous intrusions, volcanic centers, or similar features, but in this study the restricted definition will be used.

At an early stage it was found that the solar illumination azimuth had important effects on photogeologic interpretation. Siegal (1977) experimentally investigated the role of illumination azimuth in lineament analysis by simultaneously using: (a) black and white Landsat imagery covering the central Arizona area, and (b) four photographs of a plastic relief map illuminated from SE, NE, N, and NW directions for the same area at the same scale. His research showed that the number, length, coincidence, and orientation of the lineaments recognized on the photographs varied significantly. The problem of illumination-geometry biasing has also been encountered in synthetic aperture radar imagery, where it is equally troublesome (Lowman, 1992).

Sun Elevation Angle and Azimuth in Image Interpretation

Sun elevation, as usually defined for Landsat images, is the angle measured from the horizontal of sunlight at the center of a given scene. Obviously, it can also be taken as the complement of this angle, i.e., measured from the local vertical. In this study we calculated the: (a) Sun Elevation Angle (SEA), and (b) Sun Azimuth (SA) of the specific area of interest, Lesvos Island, for the 1st, 7th, and 21st day of each month of the year (Table 1). The time chosen was necessarily 0930 (local time), the time that the Landsat-5 satellite (like others, in sun-synchronous orbit) passes over Lesvos. The distribution of both SEA-values and SA-values are Gaussian (Figure 1a and 1b). The minimum SEA-value is

N.A. Soulakellis and N. Zouros are with the Department of Geography, University of the Aegean, University Hill, GR-81100 Mytilene, Greece (n.soulakellis@aegean.gr; zouros@aegean.gr).

I.D. Novak is with the Department of Geology, University of Southern Maine (novak@usm.maine.edu).

P. Lowman is with the Geodynamics Branch of NASA – Goddard Space Flight Center (Paul.D.Lowman@nasa.gov).

J. Yates is with the Geodynamics Branch of NASA – Goddard Space Flight Center (yates@core2.gsfc.nasa.gov).

Photogrammetric Engineering & Remote Sensing
Vol. 72, No. 6, June 2006, pp. 693–700.

0099-1112/06/7206–0693/$3.00/0

TABLE 1. SEASONAL VARIATION OF SUN ELEVATION ANGLE – SEA AND SUN AZIMUTH – SA FOR LESVOS ISLAND, GREECE, [LATITUDE: 39°, LONGITUDE: 26°, LOCAL TIME 9:00 AM (GMT + 2H)]

Date	Sun Elevation Angle	Sun Azimuth
1-Jan	15.03	137.64
7-Jan	15.53	137.29
21-Jan	17.51	135.84
1-Feb	19.77	134.14
7-Feb	21.21	133.03
21-Feb	24.99	129.96
1-Mar	27.63	127.67
7-Mar	29.44	126.03
21-Mar	33.65	121.85
1-Apr	36.83	118.3
7-Apr	38.48	116.3
21-Apr	41.95	111.57
1-May	44.06	108.28
7-May	45.16	106.41
21-May	47.19	102.58
1-Jun	48.25	100.35
7-Jun	48.63	99.5
21-Jun	48.98	98.69
1-Jul	48.78	99.15
7-Jul	48.48	99.83
21-Jul	47.25	102.47
1-Aug	45.75	105.35
7-Aug	44.75	107.13
21-Aug	41.91	111.63
1-Sep	39.26	115.3
7-Sep	37.68	117.29
21-Sep	33.73	121.77
1-Oct	30.77	124.76
7-Oct	28.98	126.45
21-Oct	24.9	130.04
1-Nov	21.93	132.46
7-Nov	20.44	133.62
21-Nov	17.51	135.84
1-Dec	15.99	136.95
7-Dec	15.35	137.42
21-Dec	14.71	137.88

14.71° on 21 December (winter solstice), while the maximum is 48.98° on 21 June (summer solstice). During the winter, the SEA-values vary from 14.71° to 33.65° while during summer they vary from 33.73° to 48.98°.

Sun elevation angle during the acquisition of satellite images is totally dependent, for a given latitude, on the date of image acquisition. Images recorded during winter present a significant shadow effect because of the low sun elevation, lowest on 21 December in the northern hemisphere (Lowman *et al.*, 1992). In contrast, images recorded during summer when the sun elevation is high have minimum shadowing. This results in the lack of definition of many topographic features including faults, terraces, and drainage networks.

Novak and Soulakellis (2000) acknowledged the fact that several well-known geomorphic features were neither readily identifiable nor recognizable on a digitally enhanced Landsat-5 TM image acquired in June 1990 (SEA presents their highest values) covering Lesvos Island, Greece. This was especially true for those features such as volcanic calderas which, because of their Miocene age and highly-eroded form, were not well expressed topographically.

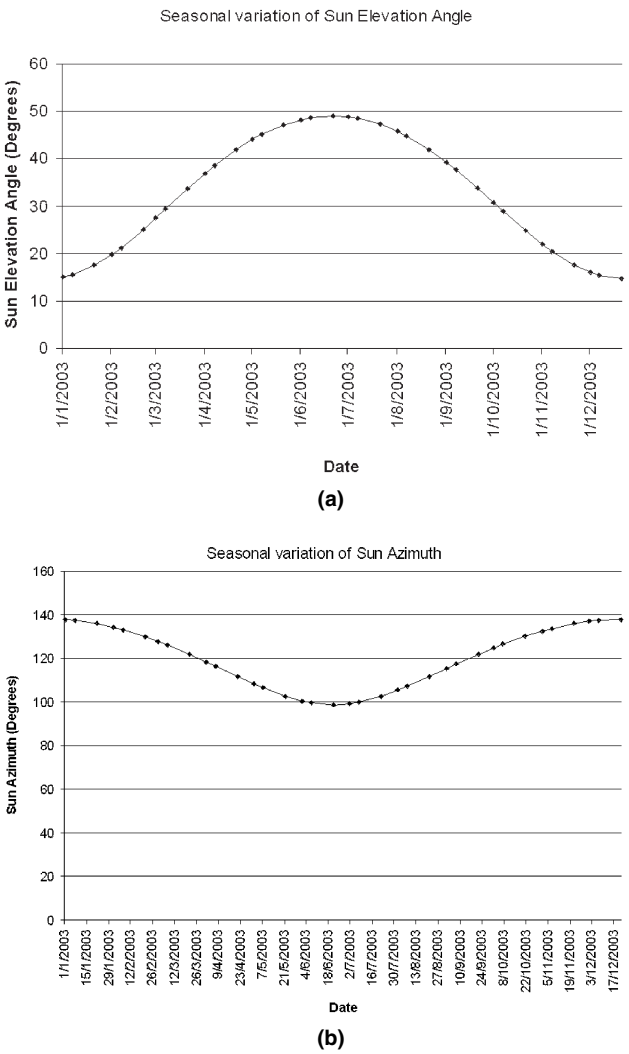

Figure 1. Graphical presentation of the seasonal variation of (a) Sun Elevation Angle, and (b) Sun Azimuth for Lesvos Island, Greece. Input parameters for the calculation were Latitude: 39°, Longitude: 26°, Local Time 0900 (GTM + 2h).

Image Fusion in Remote Sensing

Data fusion is a process dealing with data and information from multiple sources to achieve improved information for decision making (Hall, 1992). It is the aim of image fusion to integrate different data in order to obtain more information than can be derived from each of the single images alone (Pohl and Genderen, 1998). Digital image fusion is a relatively new research field at the leading edge of available technology, and it forms a rapidly developing area of research in remote sensing. Fused images may provide increased interpretation capabilities and more reliable results since data with different characteristics are combined.

Remote sensing image fusion is performed at three different levels according to the datasets at which the fusion takes place:

- Single sensor datasets, where multi-temporal (Weydahl, 1993), multi-spatial (Chiche *et al.*, 1985) or multi-spectral (Gueyenne, 1995) images have been fused in order to enhance the interpretability of the original datasets.
- Multi-sensor datasets, having different temporal, spectral and spatial characteristics has been fused leading to more accurate data (Keys *et al.*, 1990; Shen, 1990) with increased utility (Rogers and Wood, 1990).
- Remote sensing data with ancillary data, e.g., image with topographic maps or digital elevation models for improved classification purposes (Jansen *et al.*, 1990) or visualization (Toutin and Rivard, 1995).

Pohl and Van Genderen in 1998, provide the concepts, methods and applications of multi-sensor image fusion in remote sensing. According to them, fusion techniques can be grouped into the following two classes: (a) color related techniques to display single and/or multi-sensor satellite images in color, e.g., RGB, HIS, and HSV (Russ, 1995), and (b) statistical/numerical methods to provide new datasets by using mathematical combinations of image channels. It comprises addition, subtraction, multiplication and division (ratio), as well as combinations of these operations. Widely exploited fusion techniques are, for example, Principal Component Analysis (PCA), Brovey Transform (BT), Synthetic Variable Ratio, (SVR), and Ratio Enhancement (RE).

Physical Background of the Study Area

Today, the Aegean Sea is one of the most rapidly extending areas of continental crust in the world with the southern Aegean moving at about 35 mm/yr relative to Eurasia (Jackson, 1994; Reilinger *et al.*, 1997). Neogene to Recent crustal extension in the Aegean area has been generally interpreted as a result of escape tectonics, with the Anatolian and Aegean micro-plates being squeezed westwards between the Arabian and Eurasian continental blocks (Figure 2). Westward propagation of the North Anatolian Fault into the Aegean Sea during the Pliocene-Quaternary has influenced the style of extension (Armijo *et al.*, 1999).

In the Aegean area, igneous rocks of different ages and lithologies (Pe-Piper and Piper, 2002) form belts that occur in progressively younger sequences from north to south. Lesvos Island is in the northern Aegean Sea (Figure 2). It is the third largest Greek island comprising 1632 km^2, with a maximum length and width of 67 km and 45 km, respectively. Two unequal gulfs, Kalloni in the west and Gera in the east, divide the island into three parts. Both gulfs have very narrow openings to the Aegean Sea and are bounded by normal faults so that their origin is considered as a local expression of the regional extension (Figure 2).

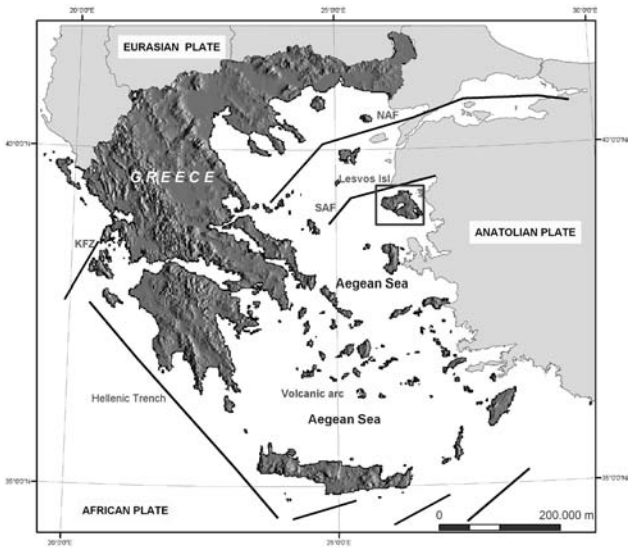

Figure 2. Simplified tectonic map of the Aegean Sea. Lesvos Island (in rectangle) is located on the North-East of Greece near the mainland of Asia Minor. Selected tectonic features shown include: NAF: North Anatolian Fault; SAF: South Anatolian Fault; KFZ: Kefalonia Fault Zone; and the Hellenic Trench and the volcanic arc.

Geology of Lesvos Island

Several studies carried out by Hecht (1972, 1973, 1974a,b, and 1975), Pe-Piper (1978), Katsikatsos *et al.* (1982, 1986), and Pe-Piper and Piper (1993) described the geology and provided the geological maps of Lesvos Island (Figure 3). The geology can be summarized as a basement composed of Alpidic and pre-Alpidic rocks which were covered later by post-Alpine formations, mainly Miocene volcanic rocks and Neogene marine and lacustrine deposits.

The geological structure of Lesvos Island has six major units:

1. An autochthonous unit of Permo-Triassic age, including mica schists, quartzites, meta-sandstones, and phyllites.
2. Two allochthonous units representing the volcano-sedimentary nappe and the ophiolitic nappe. The initial emplacement of both allochthonous units took place during Jurassic times (Papanikolaou, 1999) and they are considered remnants of an old Tethyan oceanic crust (Mountrakis *et al.*, 2001), which was obducted over the Eurasian continental margin.
3. Neogene volcanic rocks, dominating the central and western part of the island. Lesvos is part of a belt of late Oligocene: middle Miocene calc-alkaline to shoshonitic volcanism of the northern and central Aegean Sea and western Anatolia. These rocks are found in a series of heavily eroded volcanic centers along a SW-NE direction, i.e., Lepetympos, Vatousa and Agra calderas (Novak *et al.*, 2001).
4. Several volcanic rock units have been distinguished in Lesvos (Pe-Piper and Piper, 1993) ranging in age from 21.5 to 16.2 Ma. These rocks include ignimbrite, basalt, lavas, and tuffs (Pe-Piper, 1978; Borsi *et al.*, 1972).
5. Neogene marine and lacustrine deposits which comprise marls, marly limestone, silt and sandstone are present along the eastern coast of the island, as well as in Gavathas area on the northwestern coast.
6. Pleistocene and Holocene continental deposits cover the small plains formed by the main river valleys.

Neotectonic Structures and Active Tectonics of Lesvos

Fault geometry and kinematics in the Northern Aegean have been studied in detail by several authors (McKenzie, 1978). The broader region is characterized by basin and range-type topography (oriented NE-SW and NW-SE) because of a

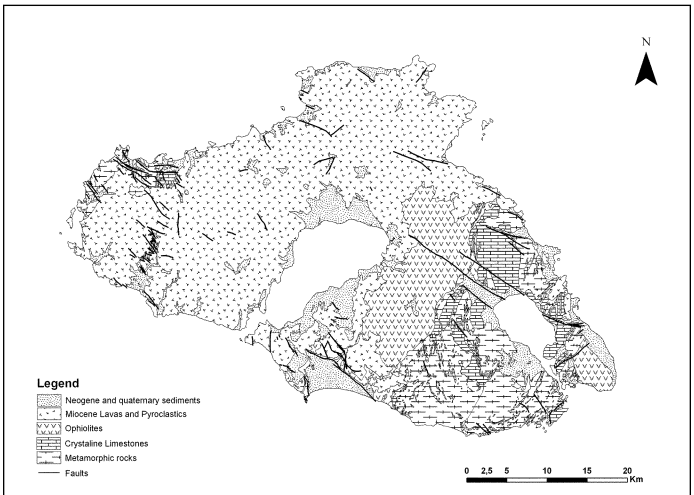

Figure 3. Simplified geologic map of Lesvos Island (from Hecht, 1971–1974).

prominent crustal extension and thinning. The role of strike–slip movements is also important due to the termination of the North Anatolian Fault along the North Anatolian Trough (Reilinger *et al.*, 2000; Meijninger, 2001; Koukouvelas and Aydin, 2002).

The North Anatolian Trough (NAT) fault system stands as a principal dextral strike-slip displacement zone while the fault pattern in the surrounding area shows mainly synthetic and antithetic shear extensional structures and rarely constructional structures. The whole tectonic regime can be interpreted as transtensional tectonics.

Lesvos Island lies south of the NAT and possesses its own rather complicated fault pattern. Lesvos reflects three different neotectonic phases, determined for the wider North Aegean area These have different directions (Mercier *et al.*, 1989; Dotsika *et al.*, 1995), which is associated with Lesvos' separation from the Asia Minor coast. These brittle fracture events, related to some very important high angle faults in kilometric scale, created the recent morphology of Lesvos Island and produced high relief depressions and grabens. The first phase occurred in Late Miocene and caused E-W to ENE-WSW trending strike-slip faults. The second phase, during the Pliocene, caused NW-SE trending normal faults, as well as NNE-SSW trending strike-slip faults. The last phase occurred during the Pleistocene in an N-S direction and created E-W trending normal faults and re-activated pre-existing structures.

Instrumental records and historic sources clearly indicate the high seismicity of Lesvos Island. Among the destructive earthquakes of the island, the most devastating was the 1867 event (estimated intensity IX to X). Based on historical manuscripts, the epicenter of this shock is believed to have been located in the central part of the island, north of Kaloni gulf. Ground fissures and associated phenomena described after the earthquake were oriented in a NNE-SSW direction. The largest known recent seismic event close to Lesvos for which a reliable fault plane solution is available, was the 19 December 1981 earthquake (M_s = 7.2, 39.2° N, 25.2° E), which seriously affected Lesvos. The fault plane solutions and the spatial distribution of aftershocks show that this fault is a dextral strike-slip fault with a normal component and has a strike of N37°E.

Data and Methodology

The main objective in this study was to minimize the uncertainty during visual interpretation of orbital images for geological and geomorphic studies by fusing them with a series of shaded relief maps.

The dataset exploited during the present study was comprised by the following digital information:

1. Landsat-5 TM satellite image of Lesvos Island, acquired on 16 August 1999, formed by 2,198 × 1,577 pixels and covering an area of approximately 66 km × 43 km. This image was extracted from a full-scene Landsat-5 TM satellite image, covering an area of 180 km × 180 km in the northern Aegean area.
2. Digital Elevation Model (DEM) of Lesvos Island with spatial resolution equal to 30 meters; it is equivalent to the spatial resolution of the Landsat-5 TM image. This DEM was generated from the digitization of the contour lines shown on four topographical maps, scale 1:50 000 (contour interval = 100 m).
3. Geologic and tectonic maps of Lesvos Island, in vector format, were generated by digitizing four geological maps, scale: 1:50 000, provided by the Institute of Geological and Mineral Exploration (IGME) of Greece.

Figure 4 presents the flow chart of the different processing stages used to generate the fused Landsat-5 TM satellite images. More analytically, the methodology followed had the following three stages:

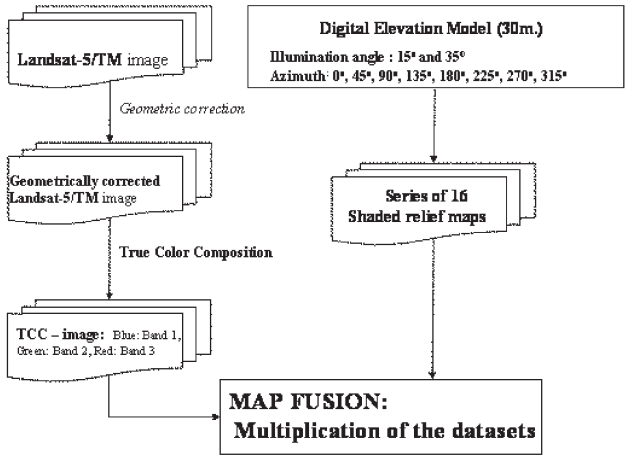

Figure 4. Flow chart of the methodology followed for producing Fused True Color Composite (FTCC) satellite images by means of original TCC image and shaded relief maps acquired by applying different illumination angles and azimuths.

Satellite Image Processing

The first stage, involves all the appropriate processes for the geometric correction and creation of a True Color Composite (TCC) satellite image. The available Landsat-5 TM satellite image, acquired on 16 August 1999, (sun elevation angle at WRS center in degrees: 43.69°; sun azimuth angle at WRS center in degrees 109.85°) was geometrically corrected by using ground control points (GCPs) with known coordinates from the topographic maps of Lesvos Island. Consequently, the geometrically corrected bands were combined to create a TCC image (Blue: band-1, Green: band-2, and Red: band-3) for preliminary visual interpretation of the geological and geomorphic features.

Series of Shaded Relief Maps Generation

The second stage involves all the appropriate processes for creating a series of sixteen (16) shaded relief maps of the study area by applying different illumination conditions on the DEM. More analytically, the DEM was used in order to produce different shaded relief maps of the island by changing both: (a) the azimuth, and (b) the illumination angle of the light source. Eight different azimuths were applied: N, NE, E, SE, S, SW, W, and NW in order to cover all the directions of lineaments and geomorphic features of the area. In tandem, two different illumination angles 15° and 35° were applied to each of the above-mentioned azimuths. The purpose was not only to examine the importance of sun elevation angles during the acquisition of the satellite images, but also to simulate the conditions of image acquisition during summer and winter, respectively.

Map Fusion

This stage involves the generation of fused image-maps by the multiplication of the two datasets created during the two previous stages. Sixteen (16) fused image-maps have been generated by applying the following equation:

$$\text{Fused images} = [\text{TCC} - \text{image}]^*[\text{Shaded Relief maps}].$$

The result of the multiplication between the two datasets was a new set of sixteen (16) fused image-maps (Figure 5) where the radiometric values of the TCC-image have been

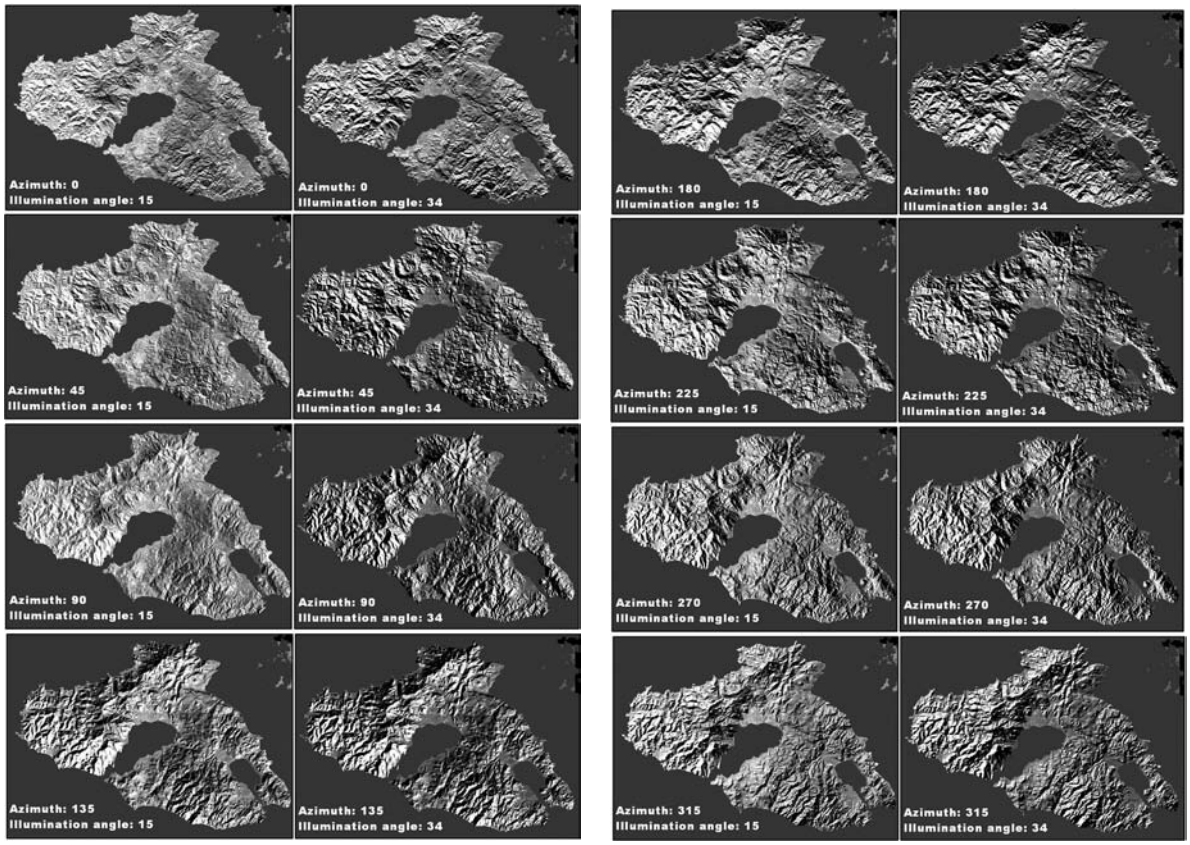

Figure 5. Grayscale version of the Fused True Color Composite (FCC) satellite images derived by fusing an original true color composite LANDSAT-5 TM image and sixteen shaded relief maps acquired by applying different illumination angles and azimuths, as shown.

modified according to the equivalent values of the shaded relief maps. This lead to a series of fused images where well-illuminated areas appear brighter and low illuminated areas appear darker than in the original TCC-image.

Fused Image-maps: Interpretation and Evaluation of the Results

The visual interpretation of the fused image-maps, generated by following the above described methodology, was carried out in two distinct stages: (a) preliminary delineation and mapping of lineaments appearing on each fused-image, and (b) synthesis of the preliminary maps, for the creation of the final lineament map of Lesvos Island and its relevant rose diagram (Figure 6).

During the first stage, the sixteen (16) fused image-maps have been interpreted independently of each other and sixteen preliminary tectonic maps were drawn. During the interpretation two main categories of lineaments were drawn: (a) lineaments, which present significant evidence of tectonic origin, and (b) lineaments, with poor appearance on each fused-map.

During the second stage, the final lineament map of Lesvos Island (see Figure 6) was created by synthesizing all of the preliminary tectonic maps. The derived map included only those lineaments that had: (a) significant presence in at least one fused image-map, and (b) poor appearance in at least one other fused image. This criterion, on which the

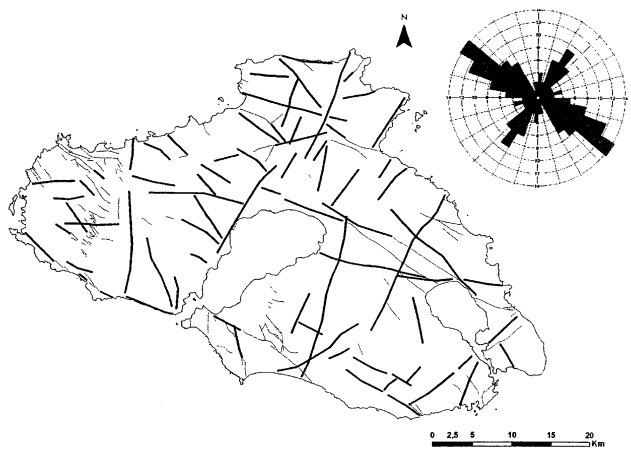

Figure 6. Lineament map of Lesvos Island derived by visual interpretation of fused satellite images. Thin lines represent mapped faults or tectonic contacts (Hecht, 1971–1974). The rose diagram of the strike directions of all lineaments shows clearly one major set of lineaments having WNW-ESE direction and one minor set having ENE-WSW direction.

synthesizing process was based, resulted in the exclusion of a small number of lineaments that had no strong evidence of tectonic origin in any of the sixteen interpreted fused images.

The evaluation of the derived results was carried out in the light of: (a) the digital geologic and tectonic map of Lesvos Island, in vector format, scale: 1:50 000 (Figure 3); (b) the digital tectonic map provided by Novak and Soulakellis in 2000, which was generated by the visual interpretation of a digital Landsat-5 TM satellite image, acquired on 20 June 1990; and (c) four "index-sites" (see Figure 7), which represent the majority of the tectonic and geomorphic features of Lesvos Island because they were specially selected according to the following criteria: (i) each has a different azimuth, (ii) each presents different morphological characteristics, and (iii) all are not easily identifiable and had not been mapped previously by means of satellite images. Two of the "index" sites are faults, named the Stypsi and Larsos faults, with NNE to SSW and ESE to WNW orientation, respectively. The third is a volcanic caldera located at the southwest part of the island, presenting a very clear circular shape, and the fourth one is a drainage basin, located at the eastern part of the island, called the Tsichliotas River basin (see Figure 7).

The Stypsi fault, at NNE-SSW, a dextral strike slip fault affecting the central part of Lesvos Island, is highly associated with the largest known recent seismic event (19 December 1981 earthquake, M_s = 7.2, 39.2°N, 25.2°E). The fault plane solutions and the spatial distribution of aftershocks show that this fault has a normal component and has a strike of N37°E. It is more clearly depicted into the fused image-maps (see Figure 7) that has been created with the shaded relief map produced by applying 135° illumination azimuth and 15° illumination angle. Additionally, the Stypsi fault appears on this fused image as a more complex fault zone, consisting of several faults that vary in length and slightly in orientation. In contrast, the least helpful fused image-maps for the identification and mapping of the Stypsi fault are the fused image-maps produced by applying: 0°, 180° and at both illumination angles.

The Larsos fault, an ESE-WNW oriented normal fault affecting the eastern part of Lesvos Island, is closely associated with a hot spring. Having a normal component, dipping to the south, it is more clearly depicted in the fused image-map created with the shaded relief map produced by applying 45° illumination azimuth and 15° illumination angle (see Figure 7). Additionally, two previously unknown linear features are depicted almost parallel to and south of Larsos fault. In the light of this observation, Larsos fault can be considered as one member of a complex fault zone. In contrast, the least useful fused images for the identification and mapping of the Larsos fault are the fused images produced by applying: 135°, 315° and at both illumination angles.

These results show clearly that low-angle illumination, perpendicular to orientation of the linear tectonic features, is the most useful condition for linear tectonic feature identification and mapping. In contrast, illumination conditions that are parallel to orientation seriously affect their appearance and their topographic representation. When comparing the above mentioned faults zones (which have a perpendicular orientation to each other) their appearance in the fused images is best shown in an illumination azimuth that is at their 45° bisector. The fused image produced by applying 90° illumination azimuth and 15° illumination angle shows that these two important fault zones are joined just above the Gulf of Kalloni in central Lesvos.

Vatousa's caldera (see Figure 7) is the most clearly identifiable geomorphic feature having a well-defined circular shape. This caldera can be accurately mapped by means of all low illumination angle fused images with each of the fused images providing a different aspect of the caldera.

The Tsichliotas River basin (oriented NE-SW in the eastern part of the island) plays an important role in that it drains the volcanic rocks of the area and erosion there is responsible for the exposure of the Petrified Forest of Lesvos (Velitzelos and Zouros, 1997). This drainage basin is clearly expressed on all of the low illumination angle fused images (see Figure 7). Despite the NE-SW orientation of the main river, its branches cover almost all the azimuths from ENE to WSW.

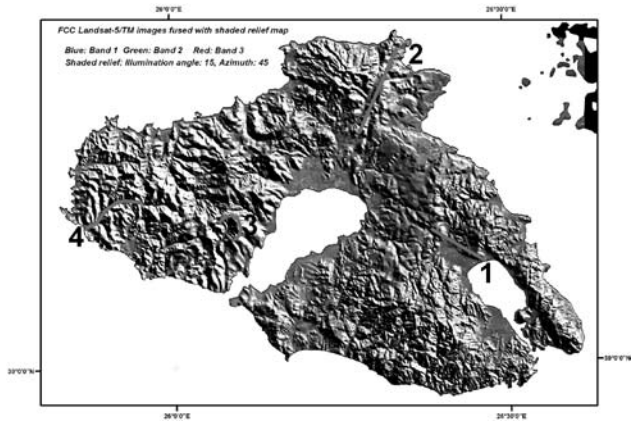

Figure 7. Four "index sites": (1) Larsos fault, a NW trending lateral fault; (2) Stipsi fault; (3) Vatousa caldera; and (4) Tsihliotas river basin as they appeared on the FCC and FFCC images (Illumination angle: 15° and azimuth: 45°).

Discussion

It is important to mention that previous studies carried out by interpreting satellite image of Lesvos for geomorphic mapping resulted in the identification and mapping of lineaments having a main NE-SW direction and a secondary NW-SE direction (Novak and Soulakellis, 2002). In contrast, the visual interpretation of the fused satellite images resulted in a new lineament map of Lesvos Island showing clearly that the main direction of the lineaments is in the WNW-ESE direction and not the NE-SW one (see Figure 6). This WNW-ESE main direction is compatible with the N-S extension stress field of the North Aegean area.

In the light of this study, this re-interpretation can best be explained by taking into consideration the fact that since the sun azimuth during satellite image acquisition over Lesvos Island varies from 98.69° to 137.88° degrees (with mean azimuth value of 121.81°), linear features associated with geological and geomorphological features that are lying perpendicular to these directions can be more easily depicted and identified. Accordingly, those which are lying parallel to sun azimuth are poorly expressed in the satellite images despite the fact that they were acquired during winter with low SEA.

Both solar elevation angle and azimuth are some of the main considerations used by image interpreters and analysts when examining multiple data sets. Our study provides another demonstration that illumination geometry is a

crucial parameter affecting the appearance of the topographically related and dependent features, and it is a significant aspect influencing image interpretability.

False color composite preparation is the "classical" image processing technique for the visual integration of multi-spectral satellite images and was a major advance in photogeology. False color image visual interpretation for identifying and mapping geological and geomorphological features is a rather complicated issue with a high degree of subjectivity. On the other hand, Digital Elevation Models (DEMs) are being increasingly exploited worldwide in geomorphic, tectonic, and geological studies. Many different approaches have been used to integrate DEMs and satellite images. The most common approach is the *"drape"* approach where an enhanced satellite image drapes over a DEM and 3D visualizations are generated.

A small portion of the reflectance (or tonal) values in satellite images is controlled by topography. The amount is dependent upon season and time of day during image acquisition. Optimally, for geologic and geomorphic investigations, low sun-angle winter images are preferred. However, winter images in this area are rarely cloud-free. Therefore, the majority of cloud-free images are acquired during high sun-angle summer months with the attendant loss of topographically related reflectance; i.e., the image appears "flat."

Traditionally, on two-dimensional topographic maps a NW to SE azimuth is applied for cartographic purposes. For full expression of topographically related tectonic or volcanic features a multi-azimuthal approach is required. This is due to the fact that geomorphological and tectonic features are poorly expressed on shaded relief maps when they lie parallel to the illumination angle. In contrast, linear features that are perpendicular to the illumination angle are clearly delineated.

Conclusions

The fusion of cloud-free, high sun-angle satellite images with azimuth-selected shaded relief maps is considered as a complementary method to improve the interpretability of such images during geomorphological and tectonic mapping. Such topographically related features include: drainage networks, drainage basins, terraces, fault traces, scarps, and volcanic landforms.

This paper has introduced a new methodology for the creation of fused images as a result of fusing original true color images with shaded relief maps. In this way, the interpretation of the resulted fused images leads to minimal uncertainty during geological and geomorphological studies. The low-illumination images reveal all the topographically related tectonic and geomorphic features. Additionally, the mutli-azimuth interpretation approach provides the opportunity to observe the interrelationships between key linear features; i.e., faults, rivers, and terraces.

Our future work includes the design and development of a 3D visualization system based on an object-oriented approach for a rapid and effective production of fused false color composite satellite images

References

Borsi, S., G. Ferrara, F. Innocenti, and R., Mazzuoli, 1972. Geochronology and petrology of recent volcanics in the Eastern Sea (West Anatolia and Lesvos Island), *Bulletin of Volcanology*, 36:473–496.

Cliche, G., F. Bonn, and P. Teillet, 1985. Integration of the SPOT Pan channel into its multispectral mode for image sharpness enhancement, *Photogrammetric Engineering & Remote Sensing*, 51:311–316.

Dotsika, E., M. Fytikas, D. Mountrakis, F. Papageorgiou, and N. Zouros, 1995. Geothermal exploration in Mytilene area (Lesvos Island, Greece), *Proceedings of the World Geothermal Congress*, Florence, Italy, 18–31 May, pp. 989–994.

Guyenne, T.-D., 1995. ERS-1/2 multi-temporal tandem image: Helsinki (Finland), *Supplement to Earth Observation Quarterly*, 48:4.

Hecht, J., 1972. *Geological Map of Lesvos Island (Plomari – Mytilene) Sheet*, 1:50 000, Greek Institute of Geology and Mineral Exploration-IGME.

Hecht, J., 1973. *Geological Map of Lesvos Island (Agia Paraskevi) Sheet*, 1:50 000, Greek Institute of Geology and Mineral Exploration-IGME.

Hecht, J., 1974a. *Geological Map of Lesvos Island (Polychnitos) Sheet*, 1:50 000, Greek Institute of Geology and Mineral Exploration-IGME.

Hecht, J., 1974b. *Geological Map of Lesvos Island (Mythimna) Sheet*, 1:50 000, Greek Institute of Geology and Mineral Exploration-IGME.

Hecht, J., 1975. *Geological Map of Lesvos Island (Eressos) Sheet*, 1:50 000, Greek Institute of Geology and Mineral Exploration-IGME.

Jackson, J.A., 1994. Active tectonics of the Aegean region, *Annual Reviews of Earth and Planetary Science*, 22:239–271.

Janssen, L.L.F., Jaarsma, M.N., and Linden, E.T.M. Van Der, 1990. Integrating topographic data with remote sensing for land-cover classification, *Photogrammetric Engineering & Remote Sensing*, 56:1503–1506.

Katsikatsos, G., D. Mataragas, G. Migiros, and E. Triantaphyllis, 1982. Geological study of Lesvos Island I.G.M.E (internal report), Athens.

Katsikatsos, G., G. Migiros, M. Triantaphyllis, and A. Mettos, 1986. Geological structure of the internal Hellinides (East Thessaly – southwest Macedonia, Euboea Attica Northern Cyclades Islands and Lesvos) I.G.M.E., *Geology and Geophysical Research*, Special issue, pp. 191–212.

Keys, L.D., N.J. Schmidt, and B.E. Phillips, 1990. A prototype example of sensor fusion used for a siting analysis, *Technical Papers 1990, ACSM-ASPRS Annual Convention, Image Processing and Remote Sensing*, 4:238–249.

Koukouvelas, I., and A. Aydin, 2002. Fault Structure and related basins of the North Aegean Sea and its surroundings, *Tectonics*, 21(5):10–17.

Lattman, L.H., 1958. Technique of mapping geologic fracture traces and lineaments on aerial photographs, *Photogrammetric Engineering & Remote Sensing*, 24:568–575.

Lowman, P., 2002. *Exploring Earth from Space: New Understanding of the Earth from Space Research*, Cambridge, Cambridge University Press, 362 pp.

Lowman, P.D., P.J. Whiting, N.M. Short, A.M. Lohmann, and G. Lee, 1992. Fracture patterns on the Canadian Shield: A lineament study with Landsat and orbital radar imagery, *Basement Tectonics*, 7:139–159.

McKenzie, D., 1978. Active tectonics of the Alpine-Himalayan belt: the Aegean Sea and surrounding regions, *Geophysical Journal of the Royal Astronomical Society*, 55:217–254.

Mercier, J.L., D. Sorel, P. Vergely, and K. Simeakis, 1989. Extensional tectonic regimes in the Aegean basins during the Cainozoic, *Basin Research*, 2:49–71.

Mountrakis, D., E. Sapountzis, A. Kilias, G. Elleftheriadis, and G. Christofides, 1983. Paleogeographic conditions in the western Pelagonian margin in Greece during the initial rifting of the continental area, *Canadian Journal Earth Science*, 20:1673–1681.

Mountrakis, D., E. Thomaidou, N. Zouros, and A. Kilias, 2001. Kinematic analysis and tertiary evolution of the Lesvos ophiolites and metamorphic sole (Aegean Sea, Greece), *Bulletin of the Geological Society of Greece*: 34(1):267–274.

Novak, I.D., and N. Soulakellis, 2000. Identifying geomorphic features using LANDSAT-5/TM data processing techniques on Lesvos, Greece, *Geomorphology Journal*, 34:101–109.

Novak, I.D., N. Soulakellis, and N. Zouros, 2001. Identifying former centers of volcanic activity on Lesvos Island, Greece, *Geological Society of America, Abstracts with Programs*, 33(6):398.

O'Leary, D.W., J.D. Friedman, and H.A. Pohn, 1976. Lineament, linear, lineation: Some proposed new standards for old terms, *Geological Society of America Bulletin*, 87:1463–1469.

Papanikolaou, D. 1999. The Triassic ophiolites of Lesvos Island within the Cimmeride orogene event, *EUG 10, Symposium D06: Inter-relations Between Paleotethys and Neotethys in Europe and Asia*, 315 p.

Pe-Piper, G., and D.J.W. Piper, 2002. *The Igneous Rocks of Greece: The Anatomy of an Orogen*, Berlin-Stuttgart, Gebrüder Borntraeger, 573 p.

Pe-Piper, G., and D.J.W. Piper, 1993. Revised stratigraphy of the Miocene volcanic rocks of Lesvos, Greece, *Neues Jahrbuch Geologie und Palaeontologie Munchen*, 2:97–110.

Pe-Piper, G. 1978. *Cainozoic Volcanic Rocks of Lesvos Island*, Ph.D. Thesis, University of Patras, 365 p.

Reilinger, R., N. Toksoz, S. McClusky, and A. Barka, 2000. Izmit-Turkey earthquake was no surprise, *GSA Today*, 10(1):1–6.

Rogers, R.H., and L. Wood, 1990. The history and status of merging multiple sensor data: An overview, *Technical Papers 1990, ACSM-ASPRS Annual Convention, Image Processing and Remote Sensing*, 4:352–360.

Russ, J.C., 1995. *The Image Processing Handbook*, Second edition, London, CRC Press.

Sarigiannis, D., N. Soulakellis, and N. Sifakis, 2004. Information fusion for computational assessment of air quality and health effects, *Photogrammetric Engineering & Remote Sensing*, 70(2):235–245.

Shen, S.S., 1990. Summary of types of data fusion methods utilized in workshop papers, *Proceedings of the Multisource Data Integration in Remote Sensing Workshop*, 14–15 June, NASA Conference Publication 3099, Greenbelt, Maryland, pp. 145–149.

Siegal, B., 1977. Izmit-Turkey earthquake was no surprise, *GSA Today*, 10(1):1–6.

Toutin, T., and B. Rivard, 1995. A new tool for depth perception of multi-source data, *Photogrammetric Engineering & Remote Sensing*, 61:1209–1211.

Velitzelos E., and N. Zouros, 1997. The petrified forest of Lesvos – Protected Natural Monument, *Proceedings of the International Symposium of I.A.E.G.*, Balkema, 3037–3043.

Weydahl, D.J., 1993. Multitemporal analysis of ERS-I SAR images over land areas, *Better Understanding of Earth Environment, Proceedings of the 13th Annual IEEE International Geoscience and Remote Sensing Symposium (IGARSS'93)*, Tokyo, Japan, 18–21 August, New York, 1459–1461.

Wise, D.U., 1974. Sub-continental sized fracture systems etched into the topography of New England, *Proceedings of the First International Conference on the New Basement Tectonics*, 4416–4221.

(Received 18 January 2003; accepted 28 February 2005; revised 28 March 2005)